Ligand Recruitment and Spin Transitions in the Solid-State Photochemistry of Fe (III) TPPCl

ARTICLE *in* THE JOURNAL OF PHYSICAL CHEMISTRY A · AUGUST 2012

Impact Factor: 2.69 · DOI: 10.1021/jp304667t · Source: PubMed

5 AUTHORS, INCLUDING:

Aaron Rury
University of Southern California
13 PUBLICATIONS **52** CITATIONS
SEE PROFILE

Roseanne J Sension
University of Michigan
108 PUBLICATIONS **2,399** CITATIONS
SEE PROFILE

THE JOURNAL OF PHYSICAL CHEMISTRY A

Article

pubs.acs.org/JPCA

Ligand Recruitment and Spin Transitions in the Solid-State Photochemistry of $Fe^{(III)}$TPPCl

Aaron S. Rury,*[,†,‡] Lauren E. Goodrich,[‡] Mary Grace I. Galinato,[§] Nicolai Lehnert,*[,‡] and Roseanne J. Sension*[,†,‡,⊥]

[†]Applied Physics Program, University of Michigan, Ann Arbor, Michigan 48109, United States

[‡]Department of Chemistry, University of Michigan, Ann Arbor, Michigan 48109, United States

[§]School of Science, Penn State Erie, The Behrend College, Erie, Pennsylvania 16563, United States

[⊥]Department of Physics, University of Michigan, Ann Arbor, Michigan 48109, United States

Supporting Information

ABSTRACT: We report evidence for the formation of long-lived photoproducts following excitation of iron(III) tetraphenylporphyrin chloride ($Fe^{(III)}$TPPCl) in a 1:1 glass of toluene and CH_2Cl_2 at 77 K. The formation of these photoproducts is dependent on solvent environment and temperature, appearing only in the presence of toluene. No long-lived product is observed in neat CH_2Cl_2 solvent. A 2-photon absorption model is proposed to account for the power-dependent photoproduct populations. The products are formed in a mixture of spin states of the central iron(III) metal atom. Metastable six-coordinate high-spin and low-spin complexes and a five-coordinate high-spin complex of iron(III) tetraphenylporphyrin are assigned using structure-sensitive vibrations in the resonance Raman spectrum. These species appear in conjunction with resonantly enhanced toluene solvent vibrations, indicating that the $Fe^{(III)}$ compound formed following photoexcitation recruits a toluene ligand from the surrounding environment. Low-temperature transient absorption (TA) measurements are used to explain the dependence of product formation on excitation frequency in this photochemical model. The six-coordinate photoproduct is initially formed in the high-spin $Fe^{(III)}$ state, but population relaxes into both high-spin and low-spin state at 77 K. This is the first demonstration of coupling between the optical and magnetic properties of an iron-centered porphyrin molecule.

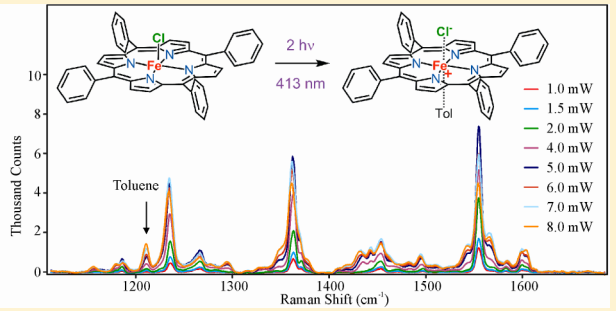

INTRODUCTION

Metalloporphyrins and their analogues are among the most extensively studied systems in chemistry.[1,2] Interest in the chemical, electronic, optical, and photochemical properties of porphyrin-ring molecules arises from their widespread application in systems that span the range from biology to molecular electronics and light harvesting. While many metalloporphyrins have been well characterized using the plethora of spectroscopic techniques available to the modern researcher, questions concerning important excited state dynamics and reactivity remain. Among these questions are the connection between optically mediated electronic transitions and the spin dynamics of the centrally ligated transition metal atoms. In particular, we would like to understand how these connections between electronic and spin transitions might be controlled.

Over the past 40 years, spin-crossover transitions in transition metal complexes have garnered intense interest.[3−7] It has been shown that varying temperature, pressure, and exposure to light can lead to changes of the spin state of several different transition metal atoms ligated in spin-crossover molecular materials.[3,5,6] The response of the magnetic moment of a molecule to temperature is the most extensively studied mechanism for inducing an atomic spin state transition. At low enough temperatures, the spin state of the atom can change due to variations in the interactions between the metal atom and its surrounding ligands.[8−11] Highly distorted six-coordinate iron(III) phorphyrins with ruffled or saddled structures exhibit spin-crossover behavior.[12−14]

In the process of developing molecular magnetic materials, researchers have found that optical interactions can couple different spin states of ligated transition metal atoms via intersystem crossing relaxation pathways. As an example of one form of the coupling of optical and magnetic properties, light-induced excited spin-state trapping (LIESST) was first demonstrated over 25 years ago in $Fe^{(II)}$-centered spin-crossover complexes.[15−17] In this form of LIESST, an optically allowed transition from the low-spin ground state produces the high-spin form of the $Fe^{(II)}$ via an intersystem crossing along a nonradiative relaxation pathway. Some studies of the dynamics

Received: May 14, 2012
Revised: June 26, 2012
Published: August 8, 2012

   dx.doi.org/10.1021/jp304667t | J. Phys. Chem. A 2012, 116, 8321−8333

of spin-crossover molecules show that this intersystem crossing occurs on subpicosecond time scales.[18] At low temperatures, steady-state light illumination at particular frequencies drives large amounts of population through the spin-crossover transition. The long lifetime of the high-spin configuration produces a photostationary state.

LIESST and similar processes coupling the optical and magnetic properties of molecules containing transition metal atoms are the basis for hundreds of studies of opto-magnetic properties of spin-crossover molecules and the development of molecular opto-magnetic materials.[19−21] However, researchers have also been left to find ways to identify, characterize and scale-up synthetic protocols for embedding inorganic light-induced spin-crossover structures into functional materials for opto-magnetic technologies. Other molecular moieties may provide a better platform from which functional magnetic molecular materials are developed.

Since metalloporphyrins represent the basic units of many chemically and photochemically efficient molecular structures in biology, a great deal of effort has gone into developing materials for catalysis, light harvesting, and molecular electronics based on metalloporphyrins. These materials range from supramolecular structures for photoinduced electron transfer,[22] to self-assembled thin films,[23] to Fe-porphyrin-like nanotube structures for oxygen reduction catalysis.[24] Recent research highlights the possibility of using metalloporphyrins for opto-magnetic technologies via selective photoassociative and dissociative channels.[25] Distorted iron(III) porphyrins exhibit anomalous spin states and magnetic behavior as a function of ligation and temperature.[12−14,26−33] Matching the suitability of metalloporphyrins for functional materials in technological devices with an ability to optically control their magnetic state may provide the necessary avenue to real-world opto-magnetic materials for biosensing, solar energy conversion, and information technology.

In the work reported here, resonance Raman and transient absorption (TA) spectroscopies are used to investigate the low-temperature excited state electronic dynamics and photochemistry of iron(III) tetraphenylporphyrin chloride [$Fe^{(III)}$TPPCl]. Raman spectra obtained with 413 nm Soret band excitation at 77 K show both a solvent and power dependence that has yet to be elucidated in the literature.[34−44] This photochemistry is also distinct from the electron transfer processes investigated with ultrafast spectroscopy in synthetic metalloporphyrins.[45−50] The power dependence in $Fe^{(III)}$TPPCl at 77 K indicates photochemistry in which at least three $Fe^{(III)}$ products are formed. The formation of all three photoproducts is well described by a 2-photon model based on light absorption from an excited electronic state with a ca. 16 ps lifetime in room temperature solution, but extended to the nanosecond time scale at 77 K.

Two features of the observed changes in the resonance Raman spectra are novel. First, the intensities of two high frequency toluene solvent vibrations show a nonlinear dependence on the incident laser power. This nonlinear power dependence indicates a resonant enhancement due to ligation of toluene by the photoexcited iron porphyrin. This phenomenon has been observed with iron porphyrins in similar, but distinctly more reactive solvent environments.[51]

Second, triplets of structure-sensitive Raman vibrations are consistent with the formation of a mixture of high-spin and low-spin six-coordinate $Fe^{(III)}$ species as well as a high-spin five-coordinate $Fe^{(III)}$ species. The low-spin six-coordinate state is populated via a spin transition through nonradiative relaxation of the initially formed six-coordinate high-spin complex. All three products appear to include coordination of at least one toluene solvent molecule. According to limits set by a quantitative model for the population, the range of possible lifetimes of this mixture of spin states is between 10 ms and 10 s. This result represents a clear demonstration of coupling between the optical and magnetic properties of an iron-centered porphyrin molecule.

EXPERIMENTAL METHODS

$Fe^{(III)}$TPPCl was synthesized using literature techniques.[52,53] Purification was achieved by column chromatography on silica, eluted first with 100% CH_2Cl_2 to remove free H_2TPP and then +5% MeOH to elute $Fe^{(III)}$TPPCl. Metalated bands were combined and then washed twice with 1 M HCl. The organic layer was dried with Na_2SO_4 and evaporated to dryness using reduced pressure.

For resonance Raman scattering measurements, 1 mM solutions of $Fe^{(III)}$TPPCl were prepared in both a 1:1 mixture of toluene and CH_2Cl_2 and neat CH_2Cl_2. These samples were pipetted into quartz electron paramagnetic resonance (EPR) tubes and immersed in liquid nitrogen in a custom homemade coldfinger apparatus, allowing the pump laser beam a clear window to the sample. Between spectra the sample EPR tube was usually moved both azimuthally and vertically such that a new portion of the sample was illuminated for each spectrum.

Resonance Raman spectra were taken with excitation in the Soret band and with excitation in the vibronic band of the Q resonances, denoted Q_v. Detailed assignments of the electronic spectrum of Fe^{III}(TPP)Cl through a combination of theoretical calculations and spectroscopic measurements have been reported by Paulat and Lehnert.[54] Wavelengths of 413.1 nm, 488.0 nm, and 514.5 nm from a Spectra Physics continuous wave Ar−Kr ion laser were used for pumping these respective transitions. Scattered light was collected with a 2 in. diameter collection lens, collimated, passed through a Kaiser Optical, Inc. holographic notch filter for rejection of both pump light and Rayleigh scattering, and then focused into a Princeton Instruments Tri-Vista Raman Spectrometer fitted with a liquid nitrogen cooled charge-coupled device (CCD) detector. The spectrometer was used in double additive mode with two 1800 gr/mm gratings for production of high-resolution spectra. Several scans, generally 8−20, were taken for each frequency window and laser power. Cosmic ray spikes were removed from the individual traces before averaging them together to produce the final spectra reported here.

Low-temperature broadband TA spectra were obtained using 1 kHz amplified femtosecond laser system. The 790 nm output of a Ti:Sapphire ultrafast oscillator (Kapteyn-Murnane Laboratories, Inc. kit) was amplified using a home-built multipass Ti:Sapphire amplifier. The resulting pulse was compressed to ca. 90 fs and split into pump and probe pulses. The pump pulse was frequency-doubled to ∼400 nm to excite the sample within the Soret resonance. The probe pulse path was lengthened by specific amounts with a precision mechanical delay stage to set the desired time delay between the arrival of the pump and probe pulses, respectively. Before reaching the sample, the probe pulse was focused into a 5 mm thick piece of CaF_2, creating a white light source stretching from 350 to 650 nm. This allowed for broadband spectral measurement of probe transmission changes of the sample in response to the excitation by the pump.

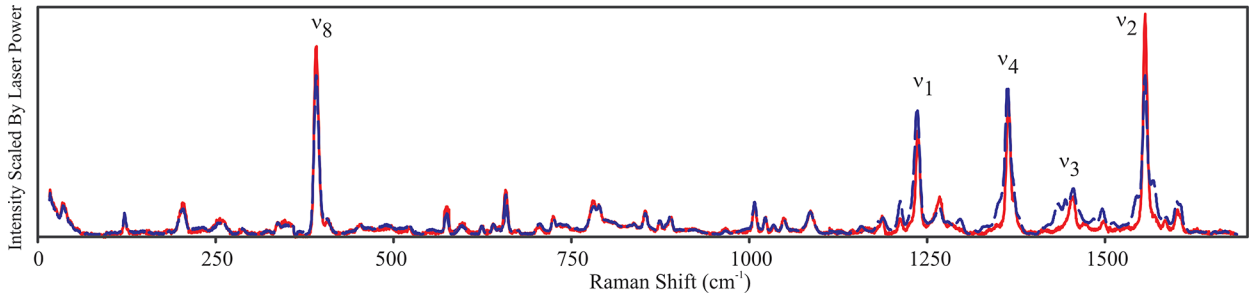

Figure 1. Parallel polarized resonance Raman scattering spectrum of $Fe^{(III)}$TPPCl in 1:1 mixture of toluene and CH_2Cl_2 at 77 K excited at 413.14 nm for two different incident laser powers, ca. 1.5 mW (red) and 7 mW (blue). The vibrational bands are labeled in Supporting Information Figure S1.

The concentration of the samples of $Fe^{(III)}$TPPCl used in the pump−probe measurements was modified to produce an optical density of between 0.5 and 1 at the pump wavelength. The samples were placed in a capped static quartz spectrophotometric cell having a 1 mm optical path length. They were cooled using a custom-built Teflon reservoir filled with liquid N_2. Cooling occurred via conduction due to contact with the reservoir. The sample was routinely cooled to −185 °C, or 88 K as measured by a thermocouple placed in the solvent. In order to reduce condensation of water vapor on the sample cell and optics, the sample and reservoir were enclosed in a Plexiglas box purged with N_2 gas dried by passage through a 25 cm tube of Drierite. Room-temperature measurements were also taken to assess the accuracy and reproducibility of this setup.

Each low-temperature difference spectrum necessitates between 1 and 2 min for collection. Between collected difference spectra, the sample cell was moved vertically to ensure that the pump and probe were overlapped in a fresh part of the sample. This helped prevent the depletion of the molecular ground state in any specific portion of the sample as the measurement was taken.

RESULTS

1. Resonance Raman Spectra. The resonance Raman spectrum of $Fe^{(III)}$TPPCl at 77 K in a 1:1 mixture of toluene and CH_2Cl_2 excited at 413.1 nm within the Soret band is plotted in Figure 1 for both high power (ca. 7 mW) and low power (ca. 1.5 mW) excitation.

The low power 413 nm Raman spectrum is dominated by the totally symmetric polarized transitions observed in the 454.5 nm spectrum reported previously.[55] However, there are some important differences. The 1235 cm^{-1} ring breathing vibration is significantly more intense. Several B_{2g} and/or B_{1g} transitions appear. Intensity is also observed in a large number of weak transitions, which may include overtones and combination bands as well as fundamental bands. Of particular note, intensity is observed in a 778 cm^{-1} band which is assigned to the overtone of the 392 cm^{-1} Fe−N breathing mode. The increase in overtone or combination modes and the appearance of nontotally symmetric B_{1g} and B_{2g} vibrational modes are consistent with an excitation wavelength near the peak of a Jahn−Teller distorted Soret excited electronic state.

Of more significance for the issues under consideration in this paper, a clear power dependence is observed in the Raman spectrum between 1100 cm^{-1} and 1700 cm^{-1}. This region contains vibrational bands sensitive to the oxidation and spin states of the iron as well as the overall charge of the porphyrin ring in well-characterized ways. This power dependence is not observed when the compound is dissolved in CH_2Cl_2 or when the excitation wavelength is 514.5 or 488.0 nm (see Supporting Information Figures S2 and S3). The power dependence observed in this spectral region with 413 nm excitation is shown in Figure 2.

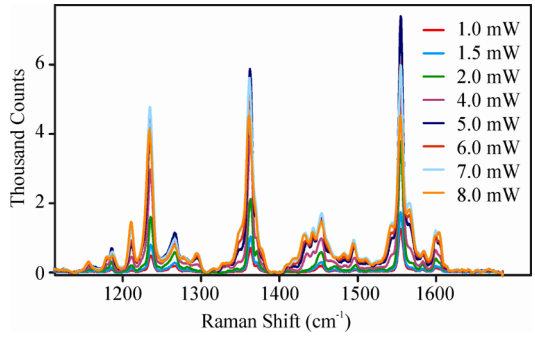

Figure 2. The spectrum of $Fe^{(III)}$TPPCl in the 1:1 mixture of toluene and CH_2Cl_2 as a function of the intensity of the excitation laser. There is clear formation of a photoproduct as the laser intensity is increased.

The strongest peak at 1556 cm^{-1}, corresponding to a combination of interior carbon ring coordinates, decreases in relative intensity as the incident laser power is increased. Along either side of this vibration appear peaks that increase in intensity as the laser power is increased. In the 1425 cm^{-1} region of the spectrum, a group of peaks appear as the laser power is increased. At lower energies, both the 1363 cm^{-1} and 1235 cm^{-1} peaks grow in intensity as the incident laser intensity is increased. There is a shoulder near 1350 cm^{-1} that grows in, as well as broadening of the peak centered at 1235 cm^{-1} accompanied by a small red-shift as power is increased. A peak at 1294 cm^{-1} also appears as power is increased.

Importantly, the photoproduct observed in the data plotted in Figures 1 and 2 does not appear to be permanent. When the intensity of the laser is reduced while remaining focused on the same area of the sample, the spectrum recovers to the spectrum obtained with low power illumination of a fresh area of the sample. In addition, the features in the spectrum are not a function of the length of the illumination time. *Thus, the data reflects formation of a photostationary mixture of ground state $Fe^{(III)}$TPPCl and photoproduct states under steady state illumination.*

Resonance Raman spectra of $Fe^{(III)}$TPPCl photoproducts following Soret band excitation have been reported in the literature. These photoproducts have been attributed primarily to iron reduction from oxygen or nitrogen-containing solvent molecules.[41,42] Certain features observed in the presence of

toluene, however, are qualitatively and quantitatively different from those reported in the literature in the presence of oxygen- or nitrogen-containing solvents. To better understand the chemical process affecting the measured spectra, resonance Raman measurements of the sample dissolved in the 1:1 mixture of toluene and CH_2Cl_2 were taken in an EPR tube washed with acetone. This leaves a small residual of acetone to interact with the sample. The power-dependent changes in the Raman spectrum when even a small amount of acetone is present are qualitatively different from that seen in Figures 1 and 2. (See Supporting Information Figure S4.)

The power-dependent spectra in the 1:1 mixture of toluene and CH_2Cl_2 can be decomposed into two different basis spectra. A singular value decomposition (SVD) algorithm was used to accomplish the separation of the spectra:[56]

$$\mathbf{A} = \mathbf{U}\cdot\mathbf{S}\cdot\mathbf{V}^{\mathrm{T}} = \mathbf{U}'\cdot\mathbf{V}^{\mathrm{T}} \quad (1)$$

where the data matrix **A** containing the Raman spectra as a function of power is decomposed into **U**, a matrix of the basis spectra, **S**, a diagonal matrix containing the singular values, and $\mathbf{V}^{\mathrm{T}}$, a matrix containing the basis amplitude vectors. Only two of the basis spectra contained significant signal, while the remaining vectors were predominantly noise (see Supporting Information Figure S5). The two basis spectra obtained from the SVD analysis are rotated to obtain physically meaningful spectra under the assumption that the spectrum obtained at the lowest power represents the linear resonance Raman spectrum of $Fe^{(III)}$TPPCl, and one of the two basis vectors should correspond to this species.

$$\mathbf{F} = \mathbf{U}'\cdot\mathbf{P}^{\mathrm{T}} \quad (2)$$

$\mathbf{U}'$ is the matrix containing the two significant basis spectra from **U**, $\mathbf{P}^{\mathrm{T}}$ is a 2×2 rotation matrix, and the matrix **F** contains the resulting basis spectra. The two basis spectra are shown in Figure 3. The spectrum labeled F_1 is essentially the spectrum

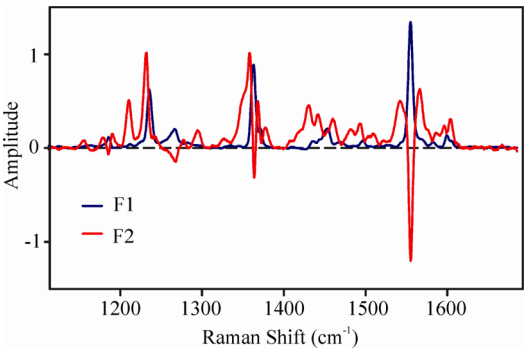

Figure 3. Spectral basis vectors obtained from the SVD. The vector F_1 from eq 2 is essentially the spectrum obtained with 1 mW excitation. The spectrum F_2 is a difference between the ground state spectrum and the photoproduct spectrum.

obtained with 1 mW excitation, while the spectrum labeled F_2 is a difference spectrum representing the conversion of $Fe^{(III)}$TPPCl into the photoproducts. As discussed below, the products include three different species. Since all three photoproducts show the same power dependence, they are all included in basis spectrum F_2.

The difference spectrum F_2 can be used to estimate the photoproduct spectrum, S_{prod} by adding the appropriate amount of the ground state spectrum F_1 back into F_2.

$$S_{\mathrm{prod}} = F_2 + \alpha F_1 \quad (3)$$

There are two clear limits constraining the value for α. (1) The product spectrum must be everywhere positive. Therefore the minimum possible value for α is the value that makes this true. (2) The spectrum obtained at the highest power used in these experiments cannot be more than 100% photoproduct. Therefore the maximum value for α is obtained by assuming that the spectrum obtained at the highest power is entirely due to the photoproduct(s). These limits for the photoproduct spectrum are compared with our best estimate of the product spectrum in Figure 4.

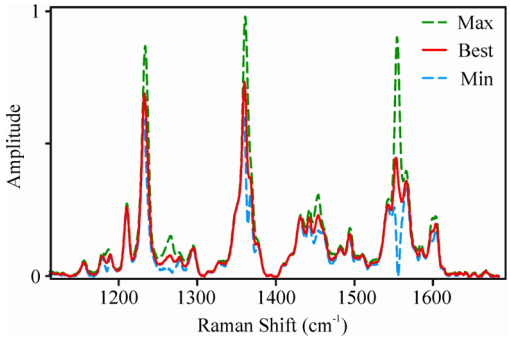

Figure 4. The photoproduct spectrum derived from the SVD analysis of the power-dependent data. The spectrum plotted in blue uses the minimum α required to ensure that the spectrum is everywhere positive. The spectrum plotted in green assumes unit conversion to photoproduct in the Raman spectrum obtained with 8 mW excitation. The spectrum plotted in red is an intermediate estimate for the photoproduct.

Most of the Raman bands observed in Figures 1, 2, and 4 are attributed to either $Fe^{(III)}$TPPCl or the photoproduct(s). However, there are a few weak transitions that arise from the 1:1 toluene:CH_2Cl_2 solvent. Of particular note, the band at 1210 cm^{-1} is a totally symmetric phenyl–methyl stretching mode of toluene. When deuterated toluene (C_7D_8) is used in the solvent mixture, this band shifts to 1174 cm^{-1}, as shown in Figure 5. This band is relatively well separated from both the $Fe^{(III)}$TPPCl vibrational bands and the photoproduct bands.

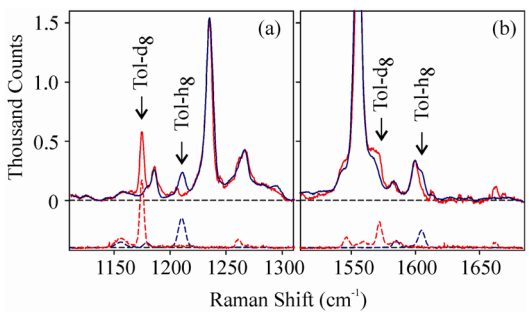

Figure 5. (a) Comparison of the spectrum of $Fe^{(III)}$TPPCl obtained with 4 mW excitation toluene (blue) or deuterated toluene (red) in the solvent. The totally symmetric phenyl–methyl stretching mode is indicated with the arrows. The solvent spectra are offset below the $Fe^{(III)}$TPPCl spectra, 1:1 CH_2Cl_2:perdeuterotoluene (red dashed) or CH_2Cl_2:toluene (blue dashed). (b) Comparison of the $Fe^{(III)}$TPPCl and solvent spectra around the 1556 cm^{-1} band. Solvent bands are also observed in this spectral region, although they are not well separated from the $Fe^{(III)}$TPPCl bands.

dx.doi.org/10.1021/jp304667t | J. Phys. Chem. A 2012, 116, 8321–8333

The totally symmetric C═C stretching band observed at 1605 cm^{-1} in toluene and 1583 cm^{-1} in deuterated toluene is also observed in the photoproduct spectrum.

The resonance enhancement of the $Fe^{(III)}$TPPCl ground state and the photoproduct(s) are not necessarily identical, and this can influence the relative intensity of the Raman bands arising from the solvent compared to those of the iron porphyrin. If the toluene bands are not resonantly enhanced, they will increase linearly with laser power and can be used to scale the relative intensity of the photoproduct to the ground state. However, the toluene bands can become enhanced if the solvent acts as a ligand to the iron and the ligand transitions are coupled to the electronic transition. Ligand bands have been observed in resonance Raman spectra of iron porphyrin compounds when the excitation wavelength is resonant with a charge transfer band.[51,57]

The toluene bands at 1210 cm^{-1} and 1605 cm^{-1} in the product spectrum can be accounted for by one of two distinct possibilities: (1) toluene acts as a ligand to the iron porphyrin in the photoproduct and appears in the spectrum because it is resonantly enhanced or (2) the resonance enhancement of the photoproduct at 413 nm is much less than that of $Fe^{(III)}$TPPCl (approximately a factor of 5 less). The decrease in the resonance enhancement of the porphyrin photoproduct would result in an increase in the relative intensity of the solvent bands. These possibilities will be discussed in greater detail in the discussion section below.

2. TA Results. The resonance Raman results presented above for $Fe^{(III)}$TPPCl in a 1:1 mixture of toluene and CH_2Cl_2 at 413 nm excitation demonstrate the existence of a photochemical pathway inaccessible with 488 or 514.5 nm excitation and unavailable when the $Fe^{(III)}$TPPCl is dissolved in neat CH_2Cl_2. Ultrafast time-resolved spectroscopy has been used to investigate the photochemical pathways in metal porphyrins and related biological hemes for over 30 years. Very little work however, has been reported for $Fe^{(III)}$TPPCl. A very early study following excitation at 353 nm indicated ultrafast ground state recovery coupled with the formation of a triplet state population with ca. 3% efficiency,[58,59] but this does not address the wavelength, solvent, or temperature dependence reported here. We therefore set out to measure the TA spectrum of $Fe^{(III)}$TPPCl at low temperature.

The polycrystalline nature of the sample in neat CH_2Cl_2 introduced scatter and precluded the measurement of the TA spectrum in this solvent at 88 K. By contrast, a nice glass formed with the 1:1 mixture of toluene and CH_2Cl_2 and allowed measurement of both the steady-state and TA spectra of this sample in a transmission geometry. TA spectra were obtained for $Fe^{(III)}$TPPCl in a 1:1 mixture of toluene and CH_2Cl_2 at 88 K and room temperature. Set time delays were used, with the probe coming before the pump and with the probe coming 0.7−0.75 fs, 50 ps, or 500 ps after the pump. The steady state absorption and the difference spectrum corresponding to a long-lived photoproduct (>∼1 ms) are plotted in Figure 6.

Of significance to the resonance Raman measurements reported above, the transient difference spectra obtained for $Fe^{(III)}$TPPCl at 88 K when the probe pulse is nominally before the excitation pulse demonstrates the accumulation of photoproducts with a lifetime >1 ms. It is likely that this difference spectrum corresponds to the photoproduct(s) observed in the Raman spectra, although the photochemical pathway must be somewhat different (*vide infra*). There is a small increase in

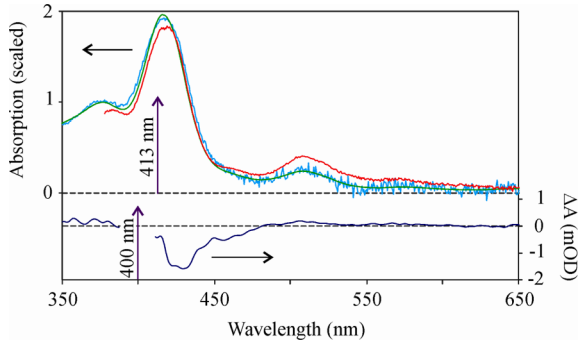

Figure 6. (Top Panel) Absorption spectra of $Fe^{(III)}$TPPCl in a 1:1 mixture of toluene and CH_2Cl_2. The spectrum plotted in green was obtained for room-temperature solution using a standard UV−vis spectrophotometer. The spectrum plotted in light blue was obtained for room-temperature solution using a femtosecond white-light continuum. The spectrum obtained at 88 K using a femtosecond white-light continuum is plotted in red. A scattering background has been subtracted from the 88 K trace. (Bottom Panel) Difference spectrum ≥ ∼1 ms following excitation of $Fe^{(III)}$TPPCl in 1:1 mixture of toluene and CH_2Cl_2 at 88K with a 400 nm pulse. This spectrum was smoothed using a 5 nm full width at half-maximum (fwhm) Gaussian to reduce pixel-to-pixel noise.

intensity in the region of the Q_v band at 507 nm and a bleaching in the region of the Soret band. Experimental factors including scattering from the pump pulse prevent accurate measurement below 400 nm, but there is no evidence for a large change in absorption in between 350 and 390 nm.

The transient spectra obtained ∼750 fs, 50 ps, and 500 ps after excitation at 400 nm in room temperature solution and in the glass at 88 K are compared in Figure 7. The room-

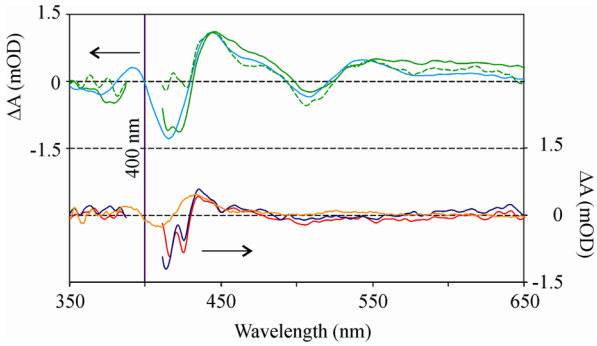

Figure 7. Comparison of the difference spectrum obtained at room temperature and at 88 K. The low-temperature difference spectra have been smoothed using a 5 nm fwhm Gaussian to reduce pixel-to-pixel noise in the spectra. The low-temperature difference spectra in two measurements at 750 and 700 fs (green) are compared to room-temperature solution (light blue) in the upper traces. The lower traces show a comparison of the difference spectra obtained at 50 ps (red) and 500 ps (blue) in the low-temperature glass with the 25 ps spectrum (orange) obtained in room-temperature solution.

temperature spectra were obtained using the same apparatus as used for the low-temperature measurements and have been scaled to match the intensity of the 88 K traces. There is a chirp to the continuum, which distorts the precise time delay at each wavelength for the ca. 750 fs measurements, but the chirp is the same for all three spectra plotted.

The room-temperature difference spectra are consistent with the previously reported data.[58,59] The behavior of the transient

dx.doi.org/10.1021/jp304667t | J. Phys. Chem. A 2012, 116, 8321−8333

difference spectrum at 88 K is similar to the behavior in room temperature solution. The spectra obtained at ca. 750 fs are essentially identical at 88 K and at room temperature. The species responsible for this spectrum decays on a picosecond time scale forming a longer-lived excited state. This longer-lived state decays back to the ground state on a time scale of ca. 16 ps in room-temperature solution. An extensive investigation of the excited state dynamics of $Fe^{(III)}$TPPCl at room temperature shows that the 16 ps decay corresponds to an electronic relaxation.[60] At 88 K the excited state persists for longer than 500 ps with no perceptible decay between 50 and 500 ps.

DISCUSSION

1. Model for the Power Dependent Raman Spectrum.

The resonance Raman scattering from $Fe^{(III)}$TPPCl in a 1:1 mixture of toluene and CH_2Cl_2 clearly shows effects due to the presence of one or more long-lived photoproduct states at low temperatures. This is confirmed by qualitative changes in the difference spectrum for different pump−probe time delays in TA measurements. The two measurements also provide information about the nature of the product formed and how it is formed in a low-temperature glass environment.

There are three key observations. First, the power-dependent resonance Raman scattering at low temperature shows a significant solvent dependence. In the polycrystalline CH_2Cl_2 environment at 77 K, the resonance Raman spectrum of $Fe^{(III)}$TPPCl shows no discernible power dependence. In the presence of toluene, however, several power-dependent features appear in the high energy spectral window of 1150−1700 cm^{-1}. This dependence on toluene seems to imply a role for solvent molecules in the formation of the photoproduct/s giving rise to the power-dependent scattering.

Second, the appearance of triplets of polarized peaks near 1555 cm^{-1} and 1445 cm^{-1} along with shoulders to both the higher and lower energy sides of the strong peak at 1363 cm^{-1} implies the existence of at least three distinct chemical products. The SVD analysis of the power-dependent spectra was able to efficiently project the data onto only two components. This leads to a separation into a component that depends approximately linearly on the laser power (the ground state of $Fe^{(III)}$TPPCl) and a component that shows a uniform nonlinear dependence on laser power. There is no evidence for additional high order processes. Thus, all three products identified by resonance Raman are produced from the same excitation process.

Third, resonance Raman scattering excited with wavelengths resonant with the transitions from the ground to Soret (413 nm) and ground to Q_v transitions (514.5 nm) provides a method to determine the dependence of the photochemical pathway on photon energy. Excitation with 8 mW at 413 nm results in a large conversion to photoproduct while excitation with 250 mW at 514.5 nm produces no photoproduct.

These observations lead to two possible models for the photochemistry of $Fe^{(III)}$TPPCl: a one-photon model or a two-photon model. In the case of a one-photon model, the excitation of the ground state forms an excited state that either returns to the ground state of the compound or produces the observed products. In the two-photon model, the excitation of the ground state forms an excited state that absorbs a second photon to produce a state from which the observed products form. These two models are sketched in Figure 8.

The low-temperature TA measurements also provide useful information. The difference spectrum observed at time delays

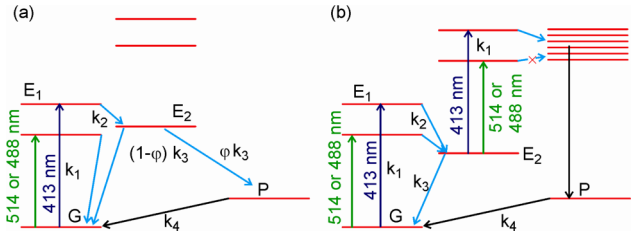

Figure 8. Schematic diagrams for the one-photon (a) or two-photon (b) photochemistry of $Fe^{(III)}$TPPCl in a 1:1 mixture of CH_2Cl_2 and toluene.

of 50 and 500 ps demonstrate the formation of a long-lived excited state with a lifetime on the order of 1 ns or longer. This excited state has an absorption spectrum with a slightly red-shifted Soret band, but displays structures and intensities otherwise similar to that of the ground state. This difference spectrum corresponds to formation of the state labeled "E_2" in Figure 8. The state "P" is either produced directly following one-photon excitation at 413 nm or following sequential two-photon excitation at 413 nm, first by the ground state and then by the E_2 excited state.

The difference spectrum observed when the probe pulse comes before the arrival of the pump pulse (bottom panel of Figure 6) corresponds to a product with a lifetime greater than 1 ms. This spectrum likely corresponds to formation of the product state "P" in Figure 8, either produced directly following one-photon excitation or following coherent two-photon excitation at 400 nm. This spectrum exhibits a decrease in the intensity on the red-side of the Soret band and an increase in the intensity of the Q_v band between 490 and 530 nm.

The data in Figure 2 can be fit to a linear combination of the ground state (GS) and product state (PS) Raman spectra. Without knowledge of the relative Raman enhancement of each species, it is impossible to be precisely quantitative in the analysis of the photochemical mechanism. Despite this limitation, the observed spectra and possible values of α in eq 3 place strict limits on the range of acceptable decompositions. Different decompositions are shown in the left-hand column of Figure 9 using the basis spectra plotted in the right-hand column. The top row uses basis spectra with relative amplitudes scaled to constant intensity in the 1210 cm^{-1} toluene band. This provides a lower limit for the relative intensity of the product spectrum and implies that this toluene band is not resonantly enhanced in the product. The middle row assumes that the integrated intensity of the three bands around 1556 cm^{-1} is equivalent to the intensity of the 1556 cm^{-1} band in the ground state spectrum. In this case, we have assumed that the resonance enhancements of the products are similar to that of the ground state molecule. The bottom row provides an example where the resonance enhancement of the product bands is approximately a factor of 3 higher than the enhancement of the ground state vibrational bands.

The populations of the states in Figure 8 can be modeled using a master equation approach to the dynamics, and the results of this analysis are compared with the observed population dependence in the left-hand column of Figure 9. For the one-photon model, the time derivatives, $\dot{n}_X(t)$, of the populations, $n_X(t)$, of each state "X" are given by:

$$\dot{n}_G(t) = -k_1 n_G(t) + k_3(1-\varphi) n_{E_2}(t) + k_4 n_P(t) \quad (4a)$$

$$\dot{n}_{E_1}(t) = k_1 n_G(t) - k_2 n_{E_1}(t) \quad (4b)$$

dx.doi.org/10.1021/jp304667t | J. Phys. Chem. A 2012, 116, 8321−8333

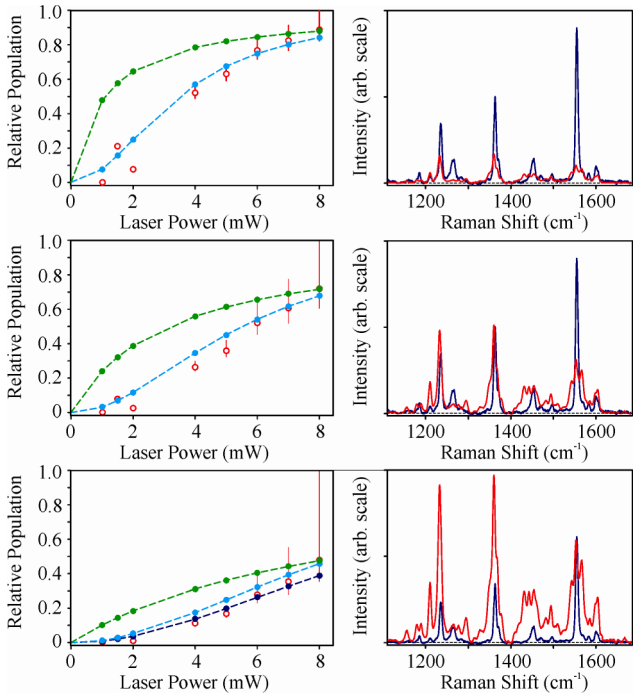

Figure 9. Comparison of the basis spectra for the ground state and photoproduct (right) and the population as a function of laser power (left) for a range of Raman enhancements of the photoproduct relative to the ground state of $Fe^{(III)}$TPPCl. The experimental populations (red with error bars) are compared with simulations using a one-photon model (green) and a two-photon model (light blue). A second two-photon calculation with a different product population at 8 mW is included for comparison in the lowest row (dark blue). The upper row assumes that the toluene bands are not resonantly enhanced in the product spectrum. This provides a lower limit for the intrinsic intensity of the photoproduct spectrum. The middle row assumes that the integrated intensity of the 1556 cm^{-1} ν_2 region is constant. The intensity of the product spectrum is approximately a factor of 3 larger than in the top row. The bottom row assumes an additional factor of 3 increase in the intensity of the photoproduct spectrum. The error bars in each plot represent the limits when the max and min product spectra in Figure 4 are used in place of the "best" product spectrum.

$$\dot{n}_{E_2}(t) = k_2 n_{E_1}(t) - k_3 n_{E_2}(t) \quad (4c)$$

$$\dot{n}_P(t) = \varphi k_3 n_{E_2}(t) - k_4 n_P(t) \quad (4d)$$

Many of the parameters in eqs 4 are constrained by the conditions of our experiments. The rate constant k_1 describes production of the electronically excited state. This rate constant depends on the number of photons absorbed per second (r_{ph}), which depends on the power of the incident laser beam (P) and the excitation frequency ($\nu = c/\lambda$), and on number of molecules in the excited volume (N). The number of molecules in the excited volume depends, in turn, on the concentration of the sample (C) and the effective volume (V) determined by the extinction coefficient at the excitation wavelength and the size of the focus.

$$k_1 = \frac{r_{ph}}{N} = \frac{P}{h\nu(CN_AV)} \quad (5)$$

The rate constant k_2 for decay of the initially excited state observed in the 750 fs difference spectra is $<\sim 1$ ps^{-1}. Since our low-temperature measurement shows that the initially excited state is not populated at 50 ps probe delay, we know k_2 must be greater than 0.02 ps^{-1} at 88 K. However, any rate constant larger than 0.02 ps^{-1} still models the data well.

The rate constant for decay of E_2 is $k_3 \leq 1$ ns^{-1}, as there is no significant decay of this state between 50 and 500 ps in the TA measurements. The rate constant k_4 for decay of the product state must be less than 1 ms^{-1} but greater than $\sim$0.1 s^{-1} since steady state is reached in the Raman measurements with an integration time on the order of minutes. The amount of product does not depend on the precise integration time.

There is a trade-off between the quantum yield for formation of the product, φ, and the rate constant for decay of the product, k_4. Assuming $k_4 = 0.1$ s^{-1}, then $\varphi \approx 10^{-4}$ to 10^{-5}. If k_4 is larger, the quantum yield will be larger as well to achieve the same steady state population.

As illustrated in Figure 9, the one-photon model does not fit the observed power dependence. This leads us to consider the two-photon model in Figure 8b with absorption from the intermediate state E_2 and photoproduct formation from a higher lying excited state. In this case, we assume that the rate constant for absorption from E_2 is the same as that for absorption from the ground state. This approximation is justified by the small ΔA observed in the TA measurements. For the two-photon model, the rate equations for the populations are

$$\dot{n}_G(t) = -k_1 n_G(t) + k_3 n_{E_2}(t) + k_4 n_P(t) \quad (6a)$$

$$\dot{n}_{E_1}(t) = k_1 n_G(t) - k_2 n_{E_1}(t) \quad (6b)$$

$$\dot{n}_{E_2}(t) = k_2 n_{E_1}(t) - k_3 n_{E_2}(t) - k_1 n_{E_2}(t) \quad (6c)$$

$$\dot{n}_P(t) = k_1 n_{E_2}(t) - k_4 n_P(t) \quad (6d)$$

As for the one-photon model, k_2 must be greater than 0.02 ps^{-1}, but the model is not sensitive to the precise value, and the rate constant, k_4, for decay of the product state must be less than 1 ms^{-1} and greater than or equal to $\sim$0.1 s^{-1}. Assuming that $k_4 =$ 0.1 s^{-1} (i.e., lifetime = 10 s) the rate constant k_3 for decay of E_2 is adjusted to match the observed data. The two-photon fits in Figure 9 result in estimates for k_3 ranging from 0.125 ns^{-1} to 0.5 ns^{-1}, i.e., the lifetime of E_2 is between 2 and 8 ns. If the lifetime of the product is shorter than 10 s (i.e. $k_4 > 0.1$ s^{-1}), the lifetime of E_2 must be longer to achieve the same steady state population. This model fits the data quite well with physically reasonable lifetimes ranging from $\tau_{E_2} = 1$ ns, $\tau_P = 10$ s to $\tau_{E_2} = 1$ μs, $\tau_P = 10$ ms. Time-dependent absorption measurements outside the time range available in our laboratory would be required to determine the lifetimes of E_2 or P more precisely.

The photochemical model put forth in Figure 8b and eqs 6 requires the assumption that the excited state responsible for product formation is not accessible with 488 or 514 nm excitation. If the state is accessible, the 250−350 mW laser power used in the experiments at these wavelengths should have produced substantial photoproduct with yields similar to those observed with 8 mW at 413 nm. Since the photochemical pathways following one-photon excitation at room temperature are independent of excitation wavelength,[60] and the difference spectra observed at low-temperature are consistent with the room temperature difference spectra, it appears that the photochemical channel is not accessible following 488 or 514 nm excitation. The photon energy at these wavelengths is not sufficient to reach the photoproduct channel from E_2.

dx.doi.org/10.1021/jp304667t | J. Phys. Chem. A 2012, 116, 8321−8333

Table 1. Summary of Vibrational Bands Undergoing Significant Changes in Frequency or Intensity in the Photoproduct[a]

			characteristic strongly polarized vibrations (a_{1g})				potentially depolarized vibrations (b_{1g}/b_{2g})	
spin			ν_3(cm^{-1})	ν_2(cm^{-1})	ν_4(cm^{-1})	ν_8(cm^{-1})	ν_{12}/ν_{27}(cm^{-1})	ϕ_s'(cm^{-1})
hs	ground state $Fe^{(III)}$TPPCl		1452	1556	1363	392	1264/1278	1494
	product spectrum	A	1431	1542	1349	392	1264	1481
		B	1442	1553	1359		1276	1494
		C	1454	1566	1372		1294	1508
ls	$[Fe^{(III)}TPP(ImH)_2]^+$ Cl^-		1459	1561	1365	(390)[b]		1501
	$[Fe^{(III)}TPP(N\text{-}MeIm)_2]^+Cl^-$[c]			1564	1369	390		
hs	$[Fe^{(III)}TPP(DMSO_2]^+$ Cl^-		1438	1541	1356			1486
	$[Fe^{(III)}TPP(DMSO_2]^+$ Cl^-[b]			1550	1360	391		
ls	$[Fe^{(II)}TPP(ImH)_2]$		1448	1557	1354	(382)[b]		1497
	$[Fe^{(II)}TPP(py)_2]$[b]			1558	1360	388	1265	1484
hs	$[Fe^{(II)}TPP(2\text{-}MeIm)]$		1431	1538	1341	(372)[b]		(1484)[b]
	$[Fe^{(II)}TPP(1,2\text{-}DiMeIm)]$[c]			1539	1344	373		

[a]A selection of comparisons with analogous compounds is also included. Unless otherwise specified, comparison frequencies are from Parthasarathi et al. JACS, 1987.[62] The spin designation indicates whether the compound is high-spin (hs) or low-spin (ls). Im = imidazole, MeIm = methylimidazole, DMSO = dimethylsulfoxide, py = pyridine. [b]Burke et al. JACS, 1978;[57] [c]Oshio et al. Spectrochim. Acta A, 1984.

2. Analysis of the Photoproduct Raman Bands. The Raman spectra of the photoproduct plotted in Figure 4 exhibit several distinct triplets of bands in the spectral region between 1100 cm^{-1} and 1700 cm^{-1}. These features are summarized in Table 1 and compared with the same bands in the spectrum of the $Fe^{(III)}$TPPCl ground state.

In contrast to the characteristic changes observed in the high-frequency region, there are no substantive changes in the low-frequency region or the mid-frequency region (see Figure 1). In particular, there is no shift in the frequency of the ν_8 totally symmetric Fe−N breathing vibration at 392 cm^{-1} as the incident laser power is increased (Raman bands here and in what follows are numbered according to the convention in Paulat et al.[55]). The relative intensity of ν_8 may decrease slightly, but no other change is observed.

The Raman spectroscopy and photochemistry of metalloporphyrins have been studied extensively over the years.[34,36,37,40,41,57,61,63−70] The vibrational bands exhibiting substantive changes in the photoproduct spectrum reported here are well-known to correlate with the oxidation state, spin state, and ligation of the iron atom in the porphyrin compound. In response to changes in the population of the different d-orbitals the metal atom may move in or out of the plane of the porphyrin ring, and the porphyrin core may expand or contract around the metal atom. These changes cause shifts in the characteristic totally symmetric Raman bands of the porphyrin ring. The bands observed in the photoproduct resonance Raman spectrum can be placed into context with a brief survey of the relevant literature.

(A). A Brief Survey of the Literature. A key study by Parthasarathi et al. compiled Raman frequencies for several iron porphyrin compounds and correlated these with the core size around the iron atom as determined by X-ray crystallography.[61] When imidazole is added to $Fe^{(III)}$TPPCl, a six-coordinate low-spin $[Fe^{(III)}TPP(ImH)_2]^+$ Cl^- complex is formed. The porphyrin center to pyrrole N distance (C_t−N) shrinks from 2.019 Å to 1.989 Å, and the vibrational frequencies increase as shown in Table 1. Similar vibrational frequencies are reported for $[Fe^{(III)}TPP(N\text{-}MeIm)_2]^+$ Cl^-.

The structure-sensitive bands of several six-coordinate high-spin $Fe^{(III)}$ porphyrins have also been studied.[61,62,71,72] In the case of $[Fe^{(III)}TPP(DMSO_2]^+$ Cl^-, the C_t−N distance increases, relative to the ground state structure of $Fe^{(III)}$TPPCl, to 2.045 Å.[61] This increase causes the structure-sensitive Raman bands to shift to lower energy, as seen in Table 1.

Reduction of the iron atom to $Fe^{(II)}$ causes the iron atom to increase in size and shift more into the plane of the porphyrin ring.[41,42,57,61,62,65,66,69] The expansion of the ring shifts the characteristic ν_2, ν_3, ν_4 and ν_8 vibrations to lower energy. Five-coordinate high-spin $Fe^{(II)}$ compounds can be formed with 2-methylimidazole or 1,2-dimethylimidazole ligands. For the $Fe^{(II)}$TPP(2-MeImH) compound, the C_t−N distance expands to 2.044 Å, and the characteristic vibrational frequencies red-shift by about 20 cm^{-1}.[61]

The six-coordinate low-spin $Fe^{(II)}$ compounds are formed with a variety of nitrogen-containing ligands including *N*-methylimidazole, pyridine, piperidine, and γ-picoline. These compounds have intermediate C_t−N distances (1.997 Å for N-MeIm) and the observed vibrational frequencies are in the same range as those observed for the high-spin $Fe^{(III)}$TPPCl compound.[57,61,62]

In addition to the characteristic shifts observed for the porphyrin breathing modes of these compounds, it is also worth noting that Spiro and Burke observed resonance enhancement of vibrational bands assigned to γ-picoline and pyridine ligands in the six-coordinate $[Fe^{(II)}\text{“XP”}(py)_2]$ and $[Fe^{(II)}\text{“XP”}(pic)_2]$ complexes upon excitation at 457.9 nm, where XP is mesoporphyrin IX or tetraphenylporphyrin.[51] The 1599 cm^{-1} and 1215 cm^{-1} bands of pyridine are strongly enhanced, while other ligand modes exhibit a weaker resonance enhancement.

Finally, we note that Evans et al. used X-ray crystallography to demonstrate the ability of benzene, toluene, and *p*-xylene to act as weak ligands to the hard metal in $[Fe^{(III)}(TPP)]^+$.[73] $Fe^{(III)}$(TPP)Y with Y being an appropriately chosen weakly coordinating anion, was dissolved in the aromatic solvent and crystallized. Crystal forces allowed biasing of the equilibrium forming crystals of $[Fe^{(III)}(TPP)(arene)]^+$ Y^-. These workers also demonstrated heptane coordination to a carefully protected $Fe^{(II)}$ porphyrin compound.[74]

(B). Assignment of the Product States. Given the information summarized above, we can assign the triplets of bands observed in the photoproduct spectrum to three distinct $Fe^{(III)}$TPP complexes, one corresponding to the red-shifted

components of the major bands (Product A), one corresponding to the blue-shifted components (Product C), and one corresponding to the components near, but not identical to, the ground state $Fe^{(III)}$TPPCl bands (Product B).

The low-frequency components of ν_2 and ν_4 corresponding to Product A are consistent with a product where the porphyrin ring expands away from the central iron. Two likely possibilities are formation of a five-coordinate high-spin $Fe^{(II)}$ species or formation of a six-coordinate high-spin $Fe^{(III)}$ species. $Fe^{(II)}$TPP(2-MeIm) and $[Fe^{(III)}TPP(DMSO_2)]^+$ Cl^- listed in Table 1 provide typical examples of such species. The absence of significant changes in the low frequency region of the spectrum casts doubt on assignment of the photoproduct to a high-spin $Fe^{(II)}$ species. There may be a modest decrease in the relative intensity of the ν_8 vibration at 392 cm^{-1}, but it is not accompanied by the appearance of a new band. The ν_8 vibration of synthetically produced high-spin $Fe^{(II)}$ species is observed at ~372 cm^{-1}.[57,62,66] By contrast, the ν_8 vibration of six-coordinate high-spin $Fe^{(III)}$ compounds remains near 390 cm^{-1}. Thus, it is likely that these bands arise from formation of a six-coordinate high-spin $Fe^{(III)}$ compound.

The central components of ν_2 and ν_4 corresponding to Product B are consistent with a high-spin $Fe^{(III)}$ species, although slightly red-shifted from the ground state values for $Fe^{(III)}$TPPCl. The position of these structure-sensitive bands implies that this product state has a structure similar to that of the ground state. These bands can be assigned to either a five-coordinate high-spin $Fe^{(III)}$ compound or a low-spin six-coordinate $Fe^{(II)}$ compound. Formation of the low-spin $Fe^{(II)}$ compound is generally accompanied by a 4 cm^{-1} to 10 cm^{-1} red-shift of the frequency of the ν_8 vibration at 392 cm^{-1}. There is no clear evidence for such a shift in the ν_8 in the data reported here. The 392 cm^{-1} band does not broaden or shift as the power of the excitation laser is increased. The only change in this band is a possible decrease in intensity. Thus the most likely assignment is to a five-coordinate high-spin $Fe^{(III)}$ compound.

The high-frequency components of ν_2 and ν_4 corresponding to Product C reflect a contraction of the porphyrin ring around the iron. These bands are consistent with the formation of a six-coordinate low-spin $Fe^{(III)}$ species or a four-coordinate $Fe^{(II)}$TPP. Early work by Spiro and co-workers showed that six-coordinate, low-spin $Fe^{(III)}$TPP complexes with a polarized band at 1568 cm^{-1} also show a polarized band at 1456 cm^{-1}.[57] This vibration is absent, however, in the four-coordinate $Fe^{(II)}$ species. The photoproducts produced from $Fe^{(III)}$TPPCl in the presence of toluene exhibits a triplet of ν_3 bands at 1454 cm^{-1}, 1442 cm^{-1}, and 1431 cm^{-1}. The appearance of a polarized band ν_3 band at 1454 cm^{-1} supports assignment of the photoproduct with a contracted porphyrin ring to a six-coordinate low-spin $Fe^{(III)}$ species rather than a four-coordinate $Fe^{(II)}$TPP.

This comparison with a range of known compounds leads to the following conclusion: *The most likely assignments for the vibrational bands observed in the photoproduct are a six-coordinate high-spin $Fe^{(III)}$ compound, a five-coordinate high-spin $Fe^{(III)}$ compound, and a six-coordinate low-spin $Fe^{(III)}$ compound.*

Fitting the vibrational bands in the 1500 cm^{-1} to 1600 cm^{-1} region of the spectrum to a sum of Gaussians provides an estimate for the relative contribution of each component to the Raman scattering: 26 ± 3% high-spin, six-coordinate; 40 ± 5% high-spin, five-coordinate; 34 ± 3% low-spin, six-coordinate (see Supporting Information Figure S6). If the resonance enhancements and the forms of the normal coordinates for all three compounds are the same, these percentages provide approximate populations. As it is likely that the resonance enhancements and the form of the normal coordinates are similar, it is reasonable to assume that the three products are formed with comparable yields, although the populations may not correspond quantitatively to the relative intensities.

(C). Photochemical Pathways and Identification of the Axial Ligands. Excitation of $Fe^{(III)}$TPPCl in a 1:1 mixture of toluene and CH_2Cl_2 at 77 K results in the formation of an excited electronic state with a lifetime greater than 1 ns, E_2 in Figure 8b. Based on the difference spectra plotted in Figure 7 this excited state has an absorption spectrum similar to that of the ground state with a slight red-shift of the Soret absorption band. Absorption of a second photon at 413 nm from this excited state accesses a photochemical pathway that is unavailable at 514.5 or 488.0 nm. This pathway results in a weakening or dissociation of the Fe−Cl bond forming reactive $Fe^{(III)}$ species that capture a nearby toluene molecule to ligate the iron atom.

The involvement of a nearby solvating toluene molecule is supported by two aspects of the measured spectra. First, the toluene bands at 1210 cm^{-1} and 1605 cm^{-1} in the photoproduct spectrum gain intensity faster than expected from a linear dependence on laser power. This demonstrates that they exhibit a resonance enhancement in the photoproduct. The 1210 cm^{-1} and 1605 cm^{-1} bands shift to lower frequencies when the solvent contains deuterated toluene as illustrated in Figure 5. This eliminates the possibility that they represent enhancement of vibrations of the phenyl groups decorating the porphyrin ring. The absence of any long-lived photoproduct in neat CH_2Cl_2 solvent corroborates the conclusion that the toluene solvent plays a crucial role in the process. Second, the pattern of enhancement of the toluene molecule implies that specific modes of the toluene molecule are enhanced in the resonance Raman spectrum of the product. The toluene bands identifiable in the lower frequency regions of the spectra shown in Figure 1 do not show a similar dependence on laser power. Enhancement of selected toluene vibrational bands in the photoproduct spectrum suggests formation of a solvent−chromophore complex. Upon formation of the complex, the solvent vibrational bands may be enhanced through excitation resonant with an excited state containing metal-to-ligand or ligand-to-metal charge transfer character.[31]

Alternatively, it is possible that the 1210 cm^{-1} and 1605 cm^{-1} vibrations of toluene are enhanced by a mechanism known as intermolecular resonance coupling that mixes the vibrations of the photoproduct chromophore with those of the surrounding solvent molecules. Veas and McHale first explained this mechanism after experimental observation of anomalous shifts in the resonance Raman spectra of porphyrin-bound oxygen and toluene solvent molecules by Kincaid and co-workers.[75,76] As a type of Fermi resonance, this intermolecular resonance coupling occurs when Raman active modes of each respective molecule are close in frequency and causes distinct shifts in the frequency of each vibration due to quantum mechanical mixing of vibrational wave functions. In response to this mixing, the higher frequency vibration shifts up in frequency while the lower frequency vibration shifts down.

In the measurements reported here, intermolecular resonance coupling in the ground state of the photoproduct may contribute to the enhancement of the 1210 cm^{-1} and 1605 cm^{-1} but is unlikely to account for the entire effect. The

vibrational modes of toluene enhanced in the photoproduct spectra do not shift from the values observed in the pure solvent within the precision of the measurements (see Figure 5), nor do any of the peaks assigned to the porphyrin product shift when the toluene is deuterated. Given that shifts in measured Raman peaks upon isotopic substitution is a tell-tale sign of intermolecular resonance coupling, we believe this mechanism does not play a large role in the enhancement of these toluene vibrations as the laser power is increased.

The X-ray crystallographic study of Evans et al. demonstrates that arenes including toluene will ligate in the axial position of $[Fe^{(III)}TPP]^+$ ions.[73] The crystal structures of $Fe^{(III)}TPP(arene)$ complexes show that two axial benzene molecules interact with the $[Fe^{(III)}TPP]^+$ core. The one with a closest Fe···C approach of 2.82 Å acts as a ligand, while the other with a closest approach of 3.18 Å is better characterized as a solvate. Toluene behaves slightly differently, with only one molecule incorporated in close proximity to the iron atom. The other face interacts with a second porphyrin in a slipped face-to-face relationship. This geometry is strongly influenced by crystal packing forces. In the low-temperature glass investigated here, $Fe^{(III)}TPPCl$ is initially in an isotropic environment. That is, there may be distortions to specific microscopic environments, but there are no systematic distortions over larger volumes of the glass. Thus the products are formed in an initially isotropic environment without crystal packing forces influencing the geometry of the complex. The vibrational frequencies of toluene are unaffected by the interaction with the Fe(III) center within the sensitivity of our measurements. This is consistent with a weak interaction and formation of a metastable complex.

In our experiments it is likely that the absorption of a photon by a molecule in the E_2 state produces a $[Fe^{(III)}TPP\cdots Cl]^{**}$ species with a weakened Fe−Cl bond. As the bond is weakened, positive charge builds up on the Fe atom, and it may ligate a surrounding toluene in the axial position opposite of that of Cl. Thus a high-spin six-coordinate compound forms in a fashion comparable to the ligation of toluene observed by Evans et al.[73]

$$Fe^{(III)}TPPCl \xrightarrow{h\nu} [Fe^{(III)}TPP^+\cdots Cl^-]^{**} \rightarrow [Fe^{(III)}TPP(Tol)^+Cl^-]$$

Similar mechanisms have been reported at room temperature in isotropic solution phase. Santha et al. reported formation of high-spin six-coordinate $[Fe^{(III)}TPP^+(1,2\text{-DiMeIm})Cl^-]$ in CH_2Cl_2 solvent.[41] Once the high-spin $[Fe^{(III)}TPP(Tol)^+Cl^-]$ compound is formed, it can expel a Cl^- forming a high-spin five-coordinate compound.

$$[Fe^{(III)}TPP(Tol)^+Cl^-] \rightarrow [Fe^{(III)}TPP(Tol)]^+ + Cl^-$$

It is also possible that the absorption of the second photon results in dissociation of the Fe−Cl bond forming $[Fe^{(III)}TPP]^+$ and a Cl^- anion. The $[Fe^{(III)}TPP]^+$ compound will then ligate a toluene from the surrounding environment in the axial position opposite of that of the dissociated Cl^- anion, forming a high-spin five-coordinate species in direct analogy to the results of Evans et al.[73]

$$Fe^{(III)}TPPCl \xrightarrow{h\nu} Fe^{(III)}TPP^+ + Cl^- \rightarrow [Fe^{(III)}TPP(Tol)^+] + Cl^-$$

Recapture of the Cl^-, or possibly a second toluene, results in the formation of a six-coordinate high-spin compound:

$$[Fe^{(III)}TPP(Tol)^+] + Cl^- \rightarrow [Fe^{(III)}TPP(Tol)^+Cl^-] \quad \text{or} \quad [Fe^{(III)}TPP^+(Tol)_2] + Cl^-$$

The available data alone cannot distinguish between a mechanism involving a weakened Fe···Cl bond and a mechanism involving photodissociation of the Fe−Cl bond. The data alone also cannot distinguish between a six-coordinate photoproduct having one toluene and one Cl^- ligand and a photoproduct with two toluene ligands. However, a product possessing a toluene ligand in each axial position is unlikely given the inability of Cl^- to move far from the coordination sphere of the Fe atom.

The products are not permanent since the Cl^- is never far from the coordination sphere of the Fe atom and does not react with toluene or CH_2Cl_2 in the solvent. A low-power measurement of the Raman spectrum following a high-power measurement on the same spot observes only ground state molecules. The barriers to reformation of $Fe^{(III)}TPPCl$ must be such that ground state recovery occurs on a time scale of milliseconds to seconds as described in connection with the two-photon model in eqs 6 above.

While power-dependent resonance Raman or ultrafast TA data cannot provide a definitive steady-state structural picture of the photoproduct states, other techniques may aid in that pursuit. Density functional theory (DFT) calculations have connected Raman spectra with ground state structures for other porphyrin systems.[55,77] At the moment, however, high-level DFT calculations may not predict vibrations of different product structures with enough accuracy to give insight into the exact nature of the formed toluene-bound photoproducts and are beyond the scope of this paper.

(D). Spin Transitions in the Photochemistry of $Fe^{(III)}TPPCl$. The mechanisms explored above account for the formation of the high-spin five-coordinate and six-coordinate products. In addition to these two products, we also observe formation of a low-spin six-coordinate compound assigned to $[Fe^{(III)}TPP(Tol)^+Cl^-]$.

Planar $Fe^{(III)}TPP$ forms six-coordinate high-spin compounds with weak axial ligands such as DMSO and six-coordinate low-spin compounds with stronger axial ligands such as imidazole. Distortions of the porphyrin ring introduce complications to this simple scheme, however. The ground electronic states of $Fe^{(III)}$ porphyrins such as $[Fe^{(III)}OEP(L_2)]ClO_4$ (where OE = octaethyl), with L = pyridine or a substituted pyridine, have shown characteristics consistent with temperature dependent quantum admixtures of high-spin $S = 5/2$ and intermediate-spin $S = 3/2$ states.[78] Several distorted saddle-shaped 6-coordinate $Fe^{(III)}$ porphyrins, including $[Fe^{(III)}OETPP(L_2)]ClO_4$, exhibit spin-crossover behavior between intermediate spin $S = 3/2$ and low-spin $S = 1/2$ states as a function of temperature when the axial ligands are pyridine or substituted pyridines.[13,14] A pure $S = 3/2$ intermediate spin state was reported for $[Fe^{(III)}OETPP(THF)_2]ClO_4$.[32] By contrast, $[Fe^{(III)}tn\text{-}OEP(py_2)](Cl \text{ or } ClO_4)$ (where *tn* = tetranitro) forms a high-spin $S = 5/2$ saddle-shaped six-coordinate complex.[33]

The photochemistry of $Fe^{(III)}TPPCl$ begins from a high-spin $Fe^{(III)}$ compound and it is expected that the initial products are formed in an electronically excited high-spin state. The ground state of the metastable product will depend on the strength of the ligands and the distortion, if any, of the porphyrin ring. From this initial high-spin excited state species, a sizable population crosses over to the low-spin six-coordinate

$[Fe^{(III)}TPP(Tol)^{+}Cl^{-}]$ state. The spin transition forming the low-spin compound likely occurs via an intersystem crossing along the nonradiative relaxation pathway of the electronically excited high-spin $[Fe^{(III)}TPP(Tol)^{+}Cl^{-}]$,[16−18] but the conversion is not complete, and the steady state product distribution contains comparable populations of both the high-spin and the low-spin species.

At least two possible mechanisms explain the accumulation of both high-spin and low-spin products. First, the additional toluene ligand bound to the Fe atom produces an increased ligand-field such that the energy necessary to pair the d-electrons is smaller than the splitting of the e_g and t_{2g} d-orbitals of the iron. After initial formation of the six-coordinate species, intersystem crossing occurs from the high- to the low-spin ground state of the molecule. Some of the population remains trapped in the high-spin configuration. A second possibility is that the six-coordinate product has an intermediate ligand field and corresponds to a spin-crossover compound. In this case, at sub-100 K temperatures, a spin equilibrium between the high- and low-spin states could be observed. Here, distortions to the porphyrin ring induced by the toluene ligand in the solid state of the solvent glass could mediate the spin transition. At these temperatures, population would then thermally equilibrate in the two spin states producing the ratios observed in our data. Each of the possibilities is examined below.

First, the ground states of many six-coordinate ferric porphyrins possess an $Fe^{(III)}$ ion in their low-spin configuration. The strong ligand field present due to the large number of bonds increases the splitting of the d-orbitals of the Fe atom. The increased splitting makes pairing the d-electrons in the t_{2g} orbitals more energetically favorable than populating the higher lying e_g orbitals. This pairing produces the low-spin configuration.

In our case, the five-coordinate species is excited to a high lying state in which the e_g orbitals are populated due to weaker ligand field splitting. This state ligates a nearby toluene molecule, forming a six-coordinate species. The ligand field splitting of this state changes such that pairing the d-electrons is energetically favorable. Therefore, electronic population crosses over to the t_{2g} orbitals producing the low-spin configuration.

Dynamically, this transition necessitates either an intersection of the potential energy surfaces of the two spin species or tunneling between the states. However, our data cannot distinguish between these two dynamical processes. If this coordination-driven mechanism accounts for the spin transition, one would need a temperature-dependent study of the relative populations of each spin state. Changes in the relative populations of the different spin states as a function of temperature would point to a crossing between energy surfaces over a barrier, while no change in the relative populations as a function of temperature would point to tunneling as the dominant mechanism for the spin transitions observed above.

However, induction of a strong ligand field by the proposed axial ligands necessitates examination of the role of this mechanism in the observed photochemistry. On one hand, toluene likely acts as a weak ligand to Fe in this product state, similar to the toluene observed by Evans et al. in an X-ray crystal structure.[73] This conclusion is also supported by the fact that the product is not permanent, even at 77 K. On the other hand, the ligand field splitting due to Cl^{-} is quite low in the spectrochemical series. In fact, Santha et al. report the room temperature formation of a high-spin, six-coordinate $Fe^{(III)}TPP$ ligated to a Cl^{-} and 1,2-dimethylimidazole in the axial positions.[31] Since toluene is a weaker ligand than 1,2-dimethylimidazole, it is possible that the room-temperature ground state of the product is a high-spin configuration, and another mechanism accounts for the spin transition.

In this second mechanism, the six-coordinate product formed after excitation is actually a spin-crossover complex where the high- and low-spin states are essentially isoenergetic. Because of this, a thermal equilibrium of spin states could then be observed at the low temperatures used for the Raman measurements. Here, the spin transition between the two states could be modulated by vibronic coupling between the d-electrons of the $Fe^{(III)}$ to the vibrations of the ligands.[8,9,11]

This possibility might also be supported by the resonance Raman spectrum of the product states. In the photoproduct spectra in Figure 4, several vibrations appear in regions where no ground state Raman active vibrations are observed. Of note are the distinct band at 1296 cm^{-1}, the two shoulders near 1330 cm^{-1} and 1315 cm^{-1}, and the two peaks between 1140 cm^{-1} and 1190 cm^{-1}. It is possible that these bands appear in the photoproduct spectrum due to symmetry lowering caused by distortions to the porphyrin ring in the presence of a toluene ligand. Lowering the symmetry of the ring increases the number of Raman active vibrations. The distortions that lead to the appearance of these bands may also account for the production of a low-spin species of the proposed photoproduct. However, Jahn−Teller distortions to the excited state participating in the resonantly enhanced scattering process may also account for the appearance of these vibrations. Our data cannot distinguish between these two mechanisms.

These mechanisms could be unraveled by a combination of optical pump-EPR or NMR probe and more extensive time-resolved optical pump, optical probe and optical pump, and Raman probe measurements as a function of temperature. The current data set provides only Raman data on the power-dependent photostationary state population.

CONCLUSION

We have presented power- and solvent-dependent resonance Raman scattering of $Fe^{(III)}TPPCl$ at 77 K via excitation in resonance with the Soret band. When the incident 413.1 nm laser power is increased, the resonance Raman scattering begins to show evidence of the presence of states of the molecule other than the ground state. SVD was used to identify the spectra of these product states.

Low-temperature TA spectroscopy was used to confirm that modest but consistent changes in absorption are observed upon excitation in the vicinity of the Soret band. The 13−18 ps lifetime of the longest-lived excited electronic state observed in room temperature ultrafast transient measurements of $Fe^{(III)}TPPCl$[60] is extended to >1 ns in the low temperature glass. Subsequent excitation of this state with 413 nm laser light accounts for the photochemistry observed in the resonance Raman measurements. The TA measurements also demonstrate the formation of a long-lived state (>1 ms) that may represent the difference spectrum for the photoproduct observed in the Raman measurements. This state shows a decrease in the red-edge of the Soret band and a slight increase in the intensity of the Q_V transition, but the spectral changes are modest with no new bands appearing in the visible region of the spectrum.

The observed photochemistry possesses two key attributes. First, we measure resonantly enhanced toluene vibrations at 1210 cm^{-1} and 1609 cm^{-1}. These vibrations are enhanced due

dx.doi.org/10.1021/jp304667t | J. Phys. Chem. A 2012, 116, 8321−8333

to ligand recruitment of toluene by the iron center in the photoproduct. Second, three sets of structure sensitive vibrations are observed, consistent with the formation of high-spin and low-spin states of a six-coordinate $Fe^{(III)}$TPP complex and a high-spin five-coordinate $Fe^{(III)}$TPP complex. The likely axial ligands of the six-coordinate species are a toluene molecule and a Cl^- anion.

Two distinct physical mechanisms could account for the formation of the low-spin state of the six-coordinate products. First, coordination of a toluene molecule may increase the ligand field splitting of the Fe d-orbitals favoring electron pairing in the lower lying t_{2g} orbitals. Second, the product complex could show an intermediate ligand field and belong to the family of spin-crossover complexes where the high- and low-spin states are essentially isoenergetic. This near degeneracy leads to thermal equilibration between the two states at sub-100 K temperatures. In the case of either mechanism for formation of the low-spin configuration, this result is the first demonstration of coupling the optical and magnetic properties of an iron-centered porphyrin molecule.

We have shown how light intensity can control the identity of ligands of $Fe^{(III)}$TPP in low-temperature environments resulting in changes in the spin state of the iron-porphyrin. With relatively modest laser powers, the percent conversion to photoproduct can approach unity. Use of an 8 mW 413 nm excitation laser focused to a beam diameter of 0.2 mm results in ca. 60% conversion to product. From this result, one can imagine a pathway to functional magnetic materials based on a photodriven change in coordination in the solid state. A high symmetry Fe-porphyrin chromophore is excited at a specific frequency to a state in which its axial ligand is weakened and the resulting Fe-porphyrin recruits a molecular ligand that binds in a single, dominant conformation to the Fe atom. The nature of the ligand can be tuned to induce a spin transition in the majority Fe-porphyrin molecules, resulting in an optically induced macroscopic spin-crossover transition. Excitation at a different frequency may be used to return the system to the original spin state.

Given the immense literature on the fabrication of functional metalloporphyrin materials for a vast array of applications, it seems reasonable to suggest that a suitable chromophore and host environment can be fabricated and investigated. The current measurements use a continuous wave laser for excitation at 413 nm. However, there are indications that coherent two-photon excitation with femtosecond pulses may produce similar long-lived photoproducts. Further work is required to demonstrate the formation of high-spin and low-spin $[Fe^{(III)}TPP(Tol)]^+Cl^-$ under these conditions. If two-photon excitation is effective, this photochemical pathway would alleviate the need to engineering an environment to elongate the lifetime of an excited electronic state. In that case, iron-centered metalloporphyrins may provide a valuable avenue toward functional opto-magnetic materials necessary in information science and technology, energy science, and biomedical applications.

■ ASSOCIATED CONTENT

Supporting Information

Figures labeling the Raman peaks in Figure 1, illustrating the Raman spectra in CH_2Cl_2, the spectra obtained with 514.5 nm excitation, photoproducts in the presence of acetone, the basis vectors from the SVD analysis, and Gaussian fit to ν_2. This material is available free of charge via the Internet at http://pubs.acs.org

■ AUTHOR INFORMATION

Corresponding Author

*E-mail: arury@umich.edu (A.S.R.); lehnertn@umich.edu (N.L.); rsension@umich.edu (R.J.S.).

Notes

The authors declare no competing financial interest.

■ ACKNOWLEDGMENTS

We would like to thank Steve Katnik for maintaining the lasers used in this study and Jian Peng for aiding in data collection of deuterated solvent resonance Raman spectra. This work was sponsored by the Department of the Defense, Defense Threat Reduction Agency (Grant HDTRA1-09-1-0005 to RS) and the National Science Foundation (CHE-0846235 to NL). The content of the information does not necessarily reflect the position or the policy of the federal government, and no official endorsement should be inferred.

■ REFERENCES

(1) Jurow, M.; Schuckman, A. E.; Batteas, J. D.; Drain, C. M. *Coord. Chem. Rev.* **2010**, *254*, 2297−2310.
(2) *The Handbook of Porphyrin Science*; Kadish, K. M.; Smith, K. M.; Guilard, R., Eds.; World Scientific: Singapore, 2011.
(3) Bousseksou, A.; Molnar, G.; Salmon, L.; Nicolazzi, W. *Chem. Soc. Rev.* **2011**, *40*, 3313−3335.
(4) Halcrow, M. A. *Chem. Soc. Rev.* **2011**, *40*, 4119−4142.
(5) Hayami, S.; Komatsu, Y.; Shimizu, T.; Kamihata, H.; Lee, Y. N. *Coord. Chem. Rev.* **2011**, *255*, 1981−1990.
(6) Munoz, M. C.; Real, J. A. *Coord. Chem. Rev.* **2011**, *255*, 2068−2093.
(7) Olguin, J.; Brooker, S. *Coord. Chem. Rev.* **2011**, *255*, 203−240.
(8) D'Avino, G.; Painelli, A.; Boukheddaden, K. *Phys. Rev. B* **2011**, *84*, 104119.
(9) Kuang, X. Y.; Morgensternbadarau, I.; Malfant, I. *Phys. Rev. B* **1993**, *47*, 5455−5458.
(10) Kuang, X. Y.; Zhou, K. W. *J. Phys. Chem. A* **2000**, *104*, 7308−7313.
(11) Sasaki, N.; Kambara, T. *J. Chem. Phys.* **1981**, *74*, 3472−3481.
(12) Ohgo, Y.; Ikeue, T.; Takahashi, M.; Takeda, M.; Nakamura, M. *Eur. J. Inorg. Chem.* **2004**, 798−809.
(13) Ikeue, T.; Ohgo, Y.; Ongayi, O.; Vicente, M. G. H.; Nakamura, M. *Inorg. Chem.* **2003**, *42*, 5560−5571.
(14) Ikeue, T.; Ohgo, Y.; Yamaguchi, T.; Takahashi, M.; Takeda, M.; Nakamura, M. *Angew. Chem., Int. Ed.* **2001**, *40*, 2617−2620.
(15) Decurtins, S.; Gutlich, P.; Kohler, C. P.; Spiering, H. *J. Chem. Soc., Chem. Commun.* **1985**, 430−432.
(16) Decurtins, S.; Gutlich, P.; Hasselbach, K. M.; Hauser, A.; Spiering, H. *Inorg. Chem.* **1985**, *24*, 2174−2178.
(17) Decurtins, S.; Gutlich, P.; Kohler, C. P.; Spiering, H.; Hauser, A. *Chem. Phys. Lett.* **1984**, *105*, 1−4.
(18) Juban, E. A.; Smeigh, A. L.; Monat, J. E.; McCusker, J. K. *Coord. Chem. Rev.* **2006**, *250*, 1783−1791.
(19) Einaga, Y. *J. Photochem. Photobiol. C: Photochem. Rev.* **2006**, *7*, 69−88.
(20) Sato, O. *J. Photochem. Photobiol. C: Photochem. Rev.* **2004**, *5*, 203−223.
(21) Sato, O.; Tao, J.; Zhang, Y. Z. *Angew. Chem., Int. Ed.* **2007**, *46*, 2152−2187.
(22) Wasielewski, M. R. *Chem. Rev.* **1992**, *92*, 435−461.
(23) Li, D. Q.; Swanson, B. I.; Robinson, J. M.; Hoffbauer, M. A. *J. Am. Chem. Soc.* **1993**, *115*, 6975−6980.
(24) Lee, D. H.; Lee, W. J.; Lee, W. J.; Kim, S. O.; Kim, Y.-H. *Phys. Rev. Lett.* **2011**, *106*, 175502.

(25) Thies, S.; Sell, H.; Schutt, C.; Bornholdt, C.; Nather, C.; Tuczek, F.; Herges, R. *J. Am. Chem. Soc.* **2011**, *133*, 16243−16250.
(26) Kouno, S.; Ikezaki, A.; Ikeue, T.; Nakamura, M. *J. Inorg. Biochem.* **2011**, *105*, 718−721.
(27) Nakamura, K.; Ikezaki, A.; Ohgo, Y.; Ikeue, T.; Neya, S.; Nakamura, M. *Inorg. Chem.* **2008**, *47*, 10299−10307.
(28) Sakai, T.; Ohgo, Y.; Hoshino, A.; Ikeue, T.; Saitoh, T.; Takahashi, M.; Nakamura, M. *Inorg. Chem.* **2004**, *43*, 5034−5043.
(29) Ikeue, T.; Ohgo, Y.; Nakamura, M. *Chem. Commun.* **2003**, 220−221.
(30) Ohgo, Y.; Neya, S.; Ikeue, T.; Takahashi, M.; Takeda, M.; Funasaki, N.; Nakamura, M. *Inorg. Chem.* **2002**, *41*, 4627−4629.
(31) Ikeue, T.; Ohgo, Y.; Saitoh, T.; Yamaguchi, T.; Nakamura, M. *Inorg. Chem.* **2001**, *40*, 3423−3434.
(32) Ikeue, T.; Saitoh, T.; Yamaguchi, T.; Ohgo, Y.; Nakamura, M.; Takahashi, M.; Takeda, M. *Chem. Commun.* **2000**, 1989−1990.
(33) Patra, R.; Bhowmik, S.; Ghosh, S. K.; Rath, S. P. *Dalton Trans.* **2010**, *39*, 5795−5806.
(34) Austin, J. C.; Bell, S. E. J.; Hester, R. E. *Chem. Phys. Lett.* **1990**, *169*, 342−346.
(35) Bartocci, C.; Maldotti, A.; Varani, G.; Battioni, P.; Carassiti, V.; Mansuy, D. *Inorg. Chem.* **1991**, *30*, 1255−1259.
(36) Hendrickson, D. N.; Kinnaird, M. G.; Suslick, K. S. *J. Am. Chem. Soc.* **1987**, *109*, 1243−1244.
(37) Hoshino, M.; Ueda, K.; Takahashi, M.; Yamaji, M.; Hama, Y. *J. Chem. Soc. Faraday Trans.* **1992**, *88*, 405−408.
(38) Jeoung, S. C.; Kim, D.; Cho, D. W. *J. Raman Spectrosc.* **2000**, *31*, 319−330.
(39) Sato, S.; Kamogawa, K.; Aoyagi, K.; Kitagawa, T. *J. Phys. Chem.* **1992**, *96*, 10676−10681.
(40) Shantha, P. K.; Saini, G. S. S.; Thanga, H. H.; Verma, A. L. *J. Raman Spectrosc.* **2003**, *34*, 315−321.
(41) Shantha, P. K.; Thanga, H. H.; Verma, A. L. *J. Raman Spectrosc.* **1998**, *29*, 997−1001.
(42) Terekhov, S. N.; Kruglik, S. G. *Chem. Phys. Lett.* **1995**, *245*, 268−272.
(43) Findsen, E. W.; Shelnutt, J. A.; Ondrias, M. R. *J. Phys. Chem.* **1988**, *92*, 307−314.
(44) Verma, A. L.; Sato, S.; Kitagawa, T. *Chem. Phys. Lett.* **1997**, *267*, 507−514.
(45) Andersson, M.; Davidsson, J.; Hammarstrom, L.; Korppi-Tommola, J.; Peltola, T. *J. Phys. Chem. B* **1999**, *103*, 3258−3262.
(46) Hayes, R. T.; Walsh, C. J.; Wasielewski, M. R. *J. Phys. Chem. A* **2004**, *108*, 2375−2381.
(47) Kang, Y. K.; Duncan, T. V.; Therien, M. J. *J. Phys. Chem. B* **2007**, *111*, 6829−6838.
(48) LeGourrierec, D.; Andersson, M.; Davidsson, J.; Mukhtar, E.; Sun, L.; Hammarstrom, L. *J. Phys. Chem. A* **1999**, *103*, 557−559.
(49) Mataga, N.; Chosrowjan, H.; Taniguchi, S. *J. Photochem. Photobiol. C* **2005**, *6*, 37−79.
(50) Petersson, J.; Eklund, M.; Davidsson, J.; Hammarstrom, L. *J. Am. Chem. Soc.* **2009**, *131*, 7940−7941.
(51) Spiro, T. G.; Burke, J. M. *J. Am. Chem. Soc.* **1976**, *98*, 5482−5489.
(52) Adler, A. D.; Longo, F. R.; Finarell., Jd; Goldmach., J; Assour, J.; Korsakof., L. *J. Org. Chem.* **1967**, *32*, 476.
(53) Adler, A. D.; Longo, F. R.; Kampas, F.; Kim, J. *J. Inorg. Nucl. Chem.* **1970**, *32*, 2443−2445.
(54) Paulat, F.; Lehnert, N. *Inorg. Chem.* **2008**, *47*, 4963−4976.
(55) Paulat, F.; Praneeth, V. K. K.; Nather, C.; Lehnert, N. *Inorg. Chem.* **2006**, *45*, 2835−2856.
(56) Henry, E. R.; Hofrichter, J. *Methods Enzymol.* **1992**, *210*, 129−192.
(57) Burke, J. M.; Kincaid, J. R.; Peters, S.; Gagne, R. R.; Collman, J. P.; Spiro, T. G. *J. Am. Chem. Soc.* **1978**, *100*, 6083−6088.
(58) Cornelius, P. A.; Steele, A. W.; Chernoff, D. A.; Hochstrasser, R. M. *Chem. Phys. Lett.* **1981**, *82*, 9−14.
(59) Liang, Y.; Negus, D. K.; Hochstrasser, R. M.; Gunner, M.; Dutton, P. L. *Chem. Phys. Lett.* **1981**, *84*, 236−240.
(60) Rury, A. New Insights Into Light Scattering. Ph.D. Dissertation, University of Michigan, 2012.
(61) Parthasarathi, N.; Hansen, C.; Yamaguchi, S.; Spiro, T. G. *J. Am. Chem. Soc.* **1987**, *109*, 3865−3871.
(62) Oshio, H.; Ama, T.; Watanabe, T.; Kincaid, J.; Nakamoto, K. *Spectrochim. Acta A* **1984**, *40*, 863−870.
(63) Fidler, V.; Ogura, T.; Sato, S.; Aoyagi, K.; Kitagawa, T. *Bull. Chem. Soc. Jpn.* **1991**, *64*, 2315−2322.
(64) Shantha, P. K.; Saini, G. S. S.; Thanga, H. H.; Verma, A. L. *J. Raman Spectrosc.* **2001**, *32*, 159−165.
(65) Jeoung, S. C.; Kim, D.; Cho, D. W.; Yoon, M. *J. Phys. Chem. A* **2000**, *104*, 4816−4824.
(66) Chottard, G.; Battioni, P.; Battioni, J. P.; Lange, M.; Mansuy, D. *Inorg. Chem.* **1981**, *20*, 1718−1722.
(67) Suslick, K. S.; Bautista, J. F.; Watson, R. A. *J. Am. Chem. Soc.* **1991**, *113*, 6111−6114.
(68) Bizet, C.; Morliere, P.; Brault, D.; Delgado, O.; Bazin, M.; Santus, R. *Photochem. Photobiol.* **1981**, *34*, 315−321.
(69) Leondiadis, L.; Momenteau, M.; Debois, A. *Inorg. Chem.* **1992**, *31*, 4691−4696.
(70) Suslick, K. S.; Watson, R. A. *Inorg. Chem.* **1991**, *30*, 912−919.
(71) Mashiko, T.; Kastner, M. E.; Spartalian, K.; Scheidt, W. R.; Reed, C. A. *J. Am. Chem. Soc.* **1978**, *100*, 6354−6362.
(72) Spiro, T. G.; Stong, J. D.; Stein, P. *J. Am. Chem. Soc.* **1979**, *101*, 2648−2655.
(73) Evans, D. R.; Fackler, N. L. P.; Xie, Z. W.; Rickard, C. E. F.; Boyd, P. D. W.; Reed, C. A. *J. Am. Chem. Soc.* **1999**, *121*, 8466−8474.
(74) Evans, D. R.; Drovetskaya, T.; Bau, R.; Reed, C. A.; Boyd, P. D. W. *J. Am. Chem. Soc.* **1997**, *119*, 3633−3634.
(75) Kincaid, J. R.; Proniewicz, L. M.; Bajdor, K.; Bruha, A.; Nakamoto, K. *J. Am. Chem. Soc.* **1985**, *107*, 6775−6781.
(76) Veas, C.; McHale, J. L. *J. Am. Chem. Soc.* **1989**, *111*, 7042−7046.
(77) Spiro, T. G.; Kozlowski, P. M.; Zgierski, M. Z. *J. Raman Spectrosc.* **1998**, *29*, 869−879.
(78) Gregson, A. K. *Inorg. Chem.* **1981**, *20*, 81−87.